

Crystallization of Mitochondrial Respiratory Complex II from Chicken Heart: a Membrane Protein Complex Diffracting to 2.0 Å.

**Li-shar Huang, Toni M. Borders, John T. Shen,
Chung-Jen Wang and Edward Berry**

**Physical Biosciences Division, Lawrence Berkeley National Laboratory
One Cyclotron Road, Berkeley CA 94720**

Running title: Crystallization of Mitochondrial Complex II

Synopsis

A multi-subunit mitochondrial membrane protein complex involved in the Krebs Cycle and respiratory chain has been crystallized in a form suitable for near-atomic resolution structure determination.

Abstract

A procedure is presented for preparation of diffraction-quality crystals of a vertebrate mitochondrial respiratory Complex II. The crystals have the potential to diffract to at least 2.0 Å with optimization of post-crystal-growth treatment and cryoprotection. This should allow determination of the structure of this important and medically relevant membrane protein complex at near-atomic resolution and provide great detail of the mode of binding of substrates and inhibitors at the two substrate-binding sites.

Keywords: Succinate dehydrogenase; respiration; protein structure; membrane protein; protein complex; respiratory enzyme; oxidoreductase; E.C. 1.3.5.1

1. Introduction. The mitochondrial respiratory chain oxidizes reduced substrates using molecular oxygen, and couples the resulting energy release to translocation of protons across the mitochondrial inner membrane. This results in an energized state residing in the transmembrane gradient of electrochemical potential of the proton ($\Delta\mu_{H^+}$) that is used to drive various endergonic processes including synthesis of ATP by the F_1-F_0 ATP synthase. In the 1960's, scientists working on resolution and reconstitution of the mitochondrial respiratory chain were able to fractionate the chain into four "complexes" (Green 1965) containing respectively NADH:ubiquinone reductase (Complex I), Succinate:ubiquinone reductase (Complex II), ubiquinol:cytochrome c oxidoreductase (Complex III), and cytochrome oxidase (Complex IV) activities. The F_1-F_0 ATP synthase is sometimes referred to as "Complex V". Detergent was required for the fractionation, as all four complexes are transmembraneous integral membrane protein assemblies. Although there is some evidence for higher-level organization into "supercomplexes" (Stroh *et al.* 2004), it appears that the four "complexes" do in fact represent organizational units and individual (multi-subunit) enzymes. The number of non-identical

subunits ranges from around 50 in the case of Complex I to only four for Complex II, with mitochondrial Complex II having 10-11 and Complex IV 13 subunits.

Complex II (Ackrell 2000; Cecchini 2003; Hagerhall 1997; Lancaster 2003) is unique in being a member of the Krebs's TCA cycle as well as the respiratory chain. A soluble preparation of "succinate dehydrogenase" could be prepared by treating mitochondrial membranes with chaotropes and/or organic solvent. The kinetics and regulatory properties of both soluble and "particulate" succinate dehydrogenase were studied extensively (Singer *et al.* 1973). The enzyme has an activated and "deactivated" state which interconvert slowly with a high activation energy. The equilibrium between the two states is affected by substrates and competitive inhibitors, phosphate, some nucleotides, and the redox state of the mitochondrial ubiquinone pool. The significance of these regulatory mechanisms is unclear, however, as the amount of activity in the mitochondrion is so high that even in the "deactivated" state SDH seems not to be rate limiting (Singer *et al.* 1973). This suggests that Complex II may be involved in regulating some other cellular process.

A number of cellular defects and myopathies are known to result from defects in respiratory chain enzymes. These are often associated with accumulation of damaged mitochondrial DNA with aging as a result of exposure to radicals produced by the oxidative machinery. On this count Complex II would appear to be immune, as all four subunits are encoded on cytoplasmic genes in higher eucaryotes. Nonetheless Complex II is involved in some cytopathies (Ackrell 2002).

A loss of Complex II (together with complexes II and IV) in neural tissues is observed in Huntington's disease. That this is directly involved in the disease, and not simply a side effect, is indicated by the fact that inhibition or genetic manipulation of Complex II leads to Huntington-like symptoms (Beal *et al.* 1993). More recently a role has been proposed for complex II in the induction of apoptosis (Albayrak *et al.* 2003). Perhaps related to this, Complex II subunits have been identified as tumor suppressors (Baysal *et al.* 2000; McDonnell *et al.* 2004; Niemann and Muller 2000) Complex II is also a target or potential target for agrochemical and clinical drugs, for example the fungicide flutolanil has recently been shown to act on complex II (Ito *et al.* 2004).

Complex II consists of four nonidentical subunits. The site where succinate is oxidized resides in a 68 kDa flavoprotein (FP; chain A), which together with a 28 kDa subunit

containing three iron-sulfur clusters (IP; chain B) make up the soluble succinate dehydrogenase. The other two subunits (C and D) are small hydrophobic "anchor" peptides, 16 and 11 kDa in the case of vertebrate complex II. It was recognized early on by some investigators (Davis and Hatefi 1971) that Complex II included a b-type cytochrome, although others suspected the cytochrome was a contaminant from complex III (Wikstrom 1973; Yu and Yu 1980). Later, homologous bacterial proteins were discovered with zero, one, or two hemes per flavin (reviewed in Hagerhall 1997; Lancaster 2001). Now it is agreed that the small anchor subunits of the mitochondrial enzyme contain one heme and the site where ubiquinone is reduced.

The α -proteobacteria have a respiratory chain that is quite similar to that of mitochondria. Among these organisms Complex II subunits A, B, C, and D have sequence identity with the human enzyme as high as 64%, 71%, 29%, and 36%, respectively. The more distantly related γ -proteobacterium *E. coli* has two homologs of Complex II (Cecchini *et al.* 2002). Of these the more closely related SQR functions like the mitochondrial enzyme to oxidize succinate in aerobic respiration, and has sequence identity with the human enzyme around 55% for both large subunits. The other *E. coli* complex, FRD, is expressed anaerobically and functions to reduce fumarate as the terminal acceptor of an anaerobic respiratory chain, and shows less sequence homology.

Low- to medium- resolution structures of both *E. coli* complexes have been determined (Iverson *et al.* 2002; Yankovskaya *et al.* 2003). However no experimentally determined structure of vertebrate Complex II, or any mitochondrial Complex II for that matter, is available. The available structure 1PB4 of yeast Complex II (Oyedotun and Lemire 2004) is derived by homology modeling based on bacterial complexes, and we feel it serves as much to emphasize the need for a mitochondrial structure as to fill that need.

We report here a reproducible procedure for purification and crystallization of Complex II from avian heart mitochondria, and preliminary cryoprotection conditions that permit diffraction to as high as 2.0 Å. Thanks in part to chicken genome projects at the University of Delaware and the Roslin Institute (Boardman *et al.* 2002), the entire sequence of all four subunits of chicken complex II are known. Sequence identity between the human and chicken proteins is 91, 90, 72, and 80% for the mature forms of the A, B, C, and D subunits, respectively. Datasets have been collected with a number of product and inhibitor compounds co-crystallized, for determining the binding mode of

these compounds. The structure has been solved by molecular replacement and is currently being refined against data to 2.2 Å.

2. Methods

2.1. Purification.

2.1.1 Detergent extraction- Mitochondria are prepared from chicken hearts essentially by the method of Smith (1967) and resuspended in buffer and Thesit detergent (C₁₂E_N; PEG 400 dodecyl ether; Fluka #17228) to give final concentrations 50 mM potassium phosphate pH 7.5 (KPi), 20 g/l protein and 30 g/l Thesit. The mixture is homogenized and incubated 30 minutes at 4°C before centrifugation.

2.1.2. TSK column- The supernate is diluted with 9 volumes cold water and applied to a column of DEAE-650S ToyoPearl TSK-gel. The column is washed with 17.5 mM KPi + 1.75 g/L Thesit, then eluted with a gradient 17.5 to 50 mM KPi, 1.75 to 5 g/L Thesit.

2.1.3. Hydroxyapatite- The fractions containing Complex II are pooled, diluted with 0.43 volumes cold water to bring the phosphate concentration to 35 mM, and applied to Ceramic Hydroxyapatite (Biorad type II 80 µm). Complex II binds weakly and is collected in the flow-through and in 10 column volumes of washing buffer (35 mM KPi, 3.5 g/l Thesit).

2.1.4. DEAE-Sepharose- These fractions are pooled and further diluted with 1 volume cold water before applying to a DEAE-Sepharose column (~60 × 2.5 cm). Complex II binds and remains bound during washing with 17.5 mM KPi, 1.75 g/l Thesit. It is eluted in a gradient 17.5-50 mM KPi with 1.75-5.0 g/l Thesit. Fractions are assayed by gel electrophoresis and visible spectra, to select fractions to pool.

2.1.5. Ammonium Sulphate Fractionation- Solid Ammonium sulfate is added to the pooled fractions to achieve 28% saturation at 4°C, and phase-separated detergent/lipids/protein is removed by centrifugation, yielding a gummy floating "pellet". The infranate is brought to 40% saturation by addition of more solid ammonium sulfate and centrifuged to yield a crisp, friable pellet (If this pellet is gummy the percentage saturation at the first step should be increased to remove more gummy stuff) which dissolves readily in 20 mM K-MOPS pH 7.2, 100 mM NaCl, 0.5 mM EDTA, 0.1 g/l DM (S-300 column buffer). Sufficient buffer is added to ensure the protein is completely dissolved, then the product is concentrated by ultrafiltration on YM-100 membrane to 10-15 ml.

2.1.6. Sephacryl S-300-This material is applied to an S-300 column 102 x 2.5 cm, equilibrated with S-300 column buffer. The column is eluted with the same buffer, recycling the effluent back to the top of the column one time for greater resolution before collecting fractions. This isolates one aggregation state, presumed to be the monomer (see **Results & Discussion**).

2.1.7 Density Gradient- Further separation of aggregated or dissociated material is achieved by concentrating to ~5 ml and loading on a glycerol density gradient of 20-40% glycerol in 20 mM TrisHCl pH 7.5, 100 mM NaCl, 0.5 mM EDTA, and 0.5 g/l dodecyl maltoside. This is centrifuged 16 hr, 45 k rpm in the Beckman 70-Ti fixed angle rotor. The colored band in the lower half of the gradient is collected, leaving some yellowish material in the upper half and a small button of pelleted material.

The collected material is concentrated and exchanged into 10 g/l octyl glucoside in 20 mM TrisHCl pH 7.5, 0.5 mM EDTA by repeated concentration in an Amicon/Millipore "Centriplus" centrifugal ultrafiltration device with a YM-100 membrane, ending with a final concentration around 0.4 - 0.8 mM (50-100 g/l protein).

2.2 Crystallization and post-crystallization treatments.

2.2.1 Crystallization- is by vapor diffusion in the sitting-drop format. To set up crystallization droplets, 15 μ l of concentrated protein in the above buffer is mixed with an equal volume of precipitant containing 0.1 M HEPES pH 7.5, 5% isopropanol, 100 g/l PEG 3350, 3 mM NaN₃, and various additives, for example 1.3 mM MgCl₂, 1.6 mM MnCl₂, and 15 ml/L PEG-400 (final concentrations) in the case of most crystals reported here. These are added from concentrated solutions to avoid excessive dilution. The sitting droplets are equilibrated against reservoirs containing the precipitant alone. The droplets are set up at room temperature and incubated at 4°C.

2.2.2 Co-crystallization- For co-crystallization with tight-binding inhibitors, water-soluble compounds are added in 2-fold molar excess from a concentrated stock solution before mixing with precipitants. Alcohol-soluble compounds are added from ethanolic stock solution before the last concentration step to avoid excessive alcohol concentrations. Compounds that have been successfully co-crystallized and for which diffraction data (2.2 to 2.5 Å) has been collected include oxaloacetate, malonate, 3-nitropropionic acid, 2-thienyltrifluoroacetone,

heptyl-hydroxy-quinoline-N-oxide, carboxin, and oxycarboxin. Crystals were also obtained with 1,2-dinitrobenzene, but diffracted to only 3.0 Å.

2.2.3. Cryoprotection- While this is still being optimized, a suitable cryoprotectant can be made by mixing one volume of the precipitant with 2/3 volume of 50% glycerol. Transfers for a few seconds each to a 50:50 mixture of the mother liquor with this cryoprotectant, then to the cryoprotectant alone, followed by immediate freezing, prevents ice formation and results in useable diffraction, with mosaicity sometimes as low as 0.4°.

2.3. Data collection and Processing- Diffraction data were collected at various protein crystallography beamlines at the ALS and SSRL. Data was processed using DENZO and reduced with SCALEPACK (Otwinowski and Minor 1997). The combination of relatively high mosaicity after freezing, a moderately long cell axis ($c \sim 290$ Å), and a tendency of the crystals to orient in the loop with the c axis perpendicular to the spindle can lead to problems with spot overlap when attempting to collect and process high resolution data. Measures being taken to alleviate this problem will be described below in the **Results and Discussion** section 3.5.

3. Results and Discussion.

3.1 Purification- Figure 1 shows SDS gel electrophoretic analysis of the preparation at the different stages. Cytochrome spectra show the Thesit extraction is quite selective for Complex II relative to the bc_1 complex and cytochrome oxidase (not shown). This is not apparent from the gel however, as Complex II is a minor component and not really visible in lanes 1-3. After the TSK-gel column the two large subunits are clearly visible, and become the main proteins present after hydroxyapatite and DEAE-Sepharose chromatography (lane 6). After further purification and heavier loading all four subunits are apparent after ammonium sulfate precipitation in lane 7. The last two steps, gel filtration (lane 8) and density gradient centrifugation (lane 9), have little effect on the gel profile but may be important for removing aggregated and dissociated complexes, further eliminating non-proteinaceous material such as Thesit and lipids, and removing minor interfering protein contaminants. Without the ammonium sulfate precipitation step

crystallization was less reproducible, and when crystals were obtained they were always embedded in a tough surface film which made mounting for data collection difficult.

3.2 Spectral characterization- Figure 2 shows visible spectra of the preparation before and after reducing with a trace of solid sodium dithionite. The spectral features are dominated by the heme, with a Soret peak at 411 nm in the oxidized form, sharpening and shifting to 422 nm upon reduction, and broad α and β peaks between 500-600 nm sharpening up at 560 and 525 nm in the reduced form. The α peak is asymmetric with a slight shoulder on the short-wavelength side, as reported also for the bovine cytochrome. The same sample of complex II was analyzed for heme by the pyridine hemochrome method (Berry and Trumpower 1987) and the results were used to put the absorption on an extinction coefficient scale and provide approximate heme-based extinction coefficients for the native protein: 16.8 mM^{-1} at 560 vs 542 nm for the dithionite-reduced protein, and 20.5 mM^{-1} at the same wavelength pair for the reduced-minus-oxidized difference spectrum. These values include the changes due to absorption by flavin and the iron-sulfur clusters, which we must assume to be present at constant stoichiometry if we use these extinction coefficients to quantitate the complex. These components absorb more in the oxidized than reduced form over most of the visible spectrum, and are responsible for the overall decrease in absorption that results in a negative difference absorbance even at the β peak of the cytochrome (Figure 2).

3.3 Aggregation state- The isolated complex was co-chromatographed with molecular weight standards on a gel filtration column (Sephacryl S-300) in the detergent dodecyl maltoside. Complex II eluted slightly behind, i.e. at a smaller molecular weight than, the dimeric cyt. *bc₁* complex of *Rhodobacter capsulatus*, which has 196 kDa of protein. This leads us to believe the complex as isolated is monomeric. Blue Native gel electrophoresis, a sensitive technique for the detection of aggregation between respiratory complexes, shows bovine Complex II to be monomeric under conditions where other respiratory proteins form supercomplexes (Stroh *et al.* 2004). The crystal packing in two different cells described below also gives no indication of a physiological multimer. This is in contrast to the *E. coli* Complex II protein, which crystallizes as a trimer which is believed to represent the functional state of the protein in the membrane (Yankovskaya *et al.* 2003).

3.4 Crystallization- When purified and crystallized as described, diffraction quality crystals are obtained with good reproducibility. The most common form of crystals is in the space group $P2_12_12_1$ with cell edges around $70 \times 84 \times 290 \text{ \AA}$. On a few occasions with slightly different conditions a second form has been obtained, with space group $P2_12_12$ and cell edges $120 \times 201 \times 68 \text{ \AA}$. Crystals of the most common form appear as flat plates, often rounded in outline making them appear discoidal. Figure 3a shows two such disks in focus, one lying flat and the other viewed edge-on. The crystals in Figure 3b have somewhat sharper edges: the crystals are actually improper hexagonal plates that become disc-like when the corner edges are rounded. The **b** and **c** axes are in the plane of the disk, with **a** corresponding to the short dimension or thickness of the disc. A ridge or crease is often visible along the middle of the disk surface (Figure 2a), this is parallel to the **b** axis. The crease presumably represents a very obtuse edge of the crystal, perhaps between the 1,0,0 and 1,0,1 facets.

Figures 3a and b show small, well-shaped crystals growing at the rim of the sitting-drop wells, one week after setup. Figures 3c and d show a larger crystal fished from the depths of its well 1 month after setup, which is more typical of the crystals used for data collection. It is also a flat plate, viewed face-on in 3c and edge-on in 3d. The mid-face ridge seen in 3c is about 30° from the spindle axis, implying the long **c** axis is 60° from the spindle, not a very good orientation for data collection. The small green circle in Figures 3c and 3d indicates the approximate diameter of the collimated beam ($100 \mu\text{m}$). With crystals of this size it is possible to collect several datasets from one crystal, with translation between to expose fresh protein each time.

Figure 4 shows a diffraction pattern from a similar crystal, in this case with the **C** axis about 45° from the spindle. This is a 1° oscillation with the **b**^{*}-**c**^{*} plane nearly perpendicular to the beam, **c**^{*} running from lower left to upper right. Diffraction is somewhat anisotropic, extending to highest resolution along the **c**^{*} axis. Some weak diffraction can be seen in that direction beyond 2.0 \AA , as shown in the upper inset of Figure 4, but not along the **b** axis (upper left and lower right corners of Figure 4) or **a** axis (not shown). Preliminary refinement of the structure using CNS (Brunger *et al.* 1998) gives B-tensor diagonal elements of +4, +16, and -20.

While we have selected one of the best images from one of the best crystals here, there is not a great deal of variability, and most of the variability we see probably results from poor reproducibility of the cryoprotection and freezing protocol rather than actual

differences in the crystals. The data for Table 1 is from a crystal frozen 20 days, and the diffraction in Figure 4 is from a crystal frozen 30 days, after setup. With care to keep the wells sealed between data collection trips, the crystals seem to be stable for at least four months, with some deterioration in diffraction toward the end of that period. This deterioration is probably due to excessive dehydration after many openings of the wells, and might be reversible by equilibration against fresh reservoir solution.

3.5 Data Collection and Processing. Table 1 lists some statistics for data reduction of one of our best data sets. The conditions used and results obtained will be further discussed below. A second table giving R_{sym} and I/σ_1 as a function of resolution is available as supplementary material for this paper.

The conditions used for collecting the diffraction pattern of Figure 4 were chosen for demonstrating the resolution limit, and are not appropriate for data collection. The closely spaced spots along the c^* axis, barely resolved in the image shown, would get closer as that axis rotates out of the plane tangent to Ewald's sphere, leading to severe overlap at a Φ angle 90° from that of the image shown. This problem is usually even more serious: the crystals tend to orient in the oval-shaped loops with their longest dimension along the spindle axis. The longest dimension of the crystal corresponds to the b axis, so this puts the c axis perpendicular to the spindle axis and thus nearly parallel to the x-ray beam for some range of Φ angles. Together with the sometimes high mosaicity obtained with our current freezing protocol, this makes spot overlap a potential problem that should be taken into account by the data collection strategy, despite the fact that a spacing of 290 Å is generally not considered problematic with modern data collection resources.

Spot overlap can be minimized by optimizing freezing conditions to minimize mosaicity, mounting the crystals properly for data collection about the c axis, using longer crystal-to-detector distances (because the diffraction pattern spreads out proportionally to distance, while the collimated diffraction beam giving rise to each spot diverges to a much lesser extent), optimizing beamline parameters to minimize spot size, and as a last resort by special measures during data processing.

We suspect the mosaicity results from distortion during freezing, although we have not yet tested an unfrozen crystal to verify this. Mosaicity may be reduced by optimizing postcrystallization treatment and/or annealing. Unlike the orthorhombic bovine cyt. bc1 crystals with which we have experience, these crystals are highly sensitive to

dehydration and loose diffraction if air-dried for a minute or so. Removing the crystal from the cold stream for even twenty seconds has resulted in degraded resolution, perhaps due to dehydration. Thus a cryoprotectant must be introduced into the crystal to reduce water activity while retaining unit cell volume. It may be that a slight increase in cell volume would give better-ordered crystals.

Collecting data around the *c* axis is especially effective for this crystal because the other two axes are quite modest in size. Unfortunately conventional goniometer arcs and κ -jigs are not useable at the end-stations we use due to close tolerances required to avoid collisions with other parts of the camera. The tendency of the crystals to align the *b* axis with the spindle can be overcome by picking up the crystal spatula-wise on a smaller loop, paying attention that the crease on the face of the crystal is perpendicular to the pin. Newly-available microfabricated crystal mounts (Thorne *et al.* 2003) may be useful here, providing a round hole of accurate size, a flat surface surrounding the hole, and rigidity to prevent bending under the weight of the crystal.

Using longer detector distance requires a larger detector surface or the use of 2Θ -offset to reach a given resolution limit. The data collection described in Table 1 was performed with crystal-to-detector distance of 400 mm, wavelength 0.97946 Å, and a (315 mm)² detector surface. The overall resolution is limited by this geometry, which records reflections only to 2.6 Å on the sides of the square and 2.0 in the corners. The poor completeness in the last shell, while R_{sym} and I/σ_1 still suggests useable data quality, is due to this geometry and not to rejection of weak spots: the default cut-off of -3σ was used for rejecting weak spots. Completeness is 100% in the shell 4.1 - 3.74 Å, and 97.6% for 99 - 2.6 Å.

Beamline parameter adjustments that we are looking at for minimizing spot size include focusing the beam at the detector surface or somewhere between the crystal and detector (rather than at the crystal) and closing down the slits determining the horizontal divergence of the beam.

Data processing measures to minimize overlap include carefully crafting the integration "box" to measure background on both sides of the row of closely spaced spots (not trying to use any background area between spots), and when all else fails assuming an artificially low mosaicity during integration (and not post-refining that value when scaling). This latter technique ("profile peak sampling") is necessary when the *c** axis is parallel to the beam so that the *h*, *k*, *l* and *h*, *k*, *l*+1 spots are essentially superimposed, and the mosaicity is such that their diffraction conditions overlap as a

function of Φ . By assuming a smaller mosaicity we force the integration program to measure intensity in a few frames around the peak of each reflection's diffraction condition, cutting off the wings that overlap and ignoring the fact that part of the intensity measured is due to overlap from neighboring reflections along the c^* axis.

In the case of the data collection described in Table 1 the c axis was nearly perpendicular (80°) to the spindle axis, however the mosaicity was unusually low (0.596° ; from post-refinement of data collected assuming 0.7°), and by reintegrating with an assumed mosaicity of 0.5° we were able to achieve the indicated completeness, limited mainly by the edges of the detector, with no significant increase in R_{sym} . The actual R_{sym} values are surprisingly high even in the low-resolution shells (0.096 in $99\text{-}4.71$ Å), however this is not due to integrating with underestimated mosaicity, as similar R-merge values were obtained assuming mosaicity 0.7° or even 1.5° . It is also not due to anomalous scattering from the abundant iron in this protein, as scaling Bivoet mates separately did not decrease chi-squared values. It may be due to overlap of intensity from one spot into the next spots profile - clearly if a weak spot is next to a very strong spot along the c axis, its profile will be affected significantly.

3.6 Phasing and model building. The crystals were solved by molecular replacement using the structure of the *E. coli* SDH complex (PDB entry 1NEK) as search model. After we succeeded in lowering the R-factor below 0.40 by manual rebuilding in the poorly phased density maps, the ARP/wARP procedure (Perrakis *et al.* 2001) was able to improve phases and build most of the model, as well as providing excellent maps for building the difficult parts. At present all but 23 residues out of 1117 have been built, and the model is being refined against 2.2 Å data with present R_{free}/R at $0.27/0.24$ before adding solvent. There is density at the substrate and quinone sites consistent with oxaloacetate and ubiquinone, although other occupants cannot be ruled out at this resolution and stage of refinement. Strands of density, presumably due to phospholipids and perhaps the polyprenyl side-chain of ubiquinone, are present in the membrane domain.

3.7 Crystal packing. There is one monomer (hetero-tetramer) in the asymmetric unit of the $P2_12_12_1$ crystal, giving a Matthews' coefficient of 3.47 and solvent content about 64%. The packing is illustrated in Figure 5 and shows that the crystals are of Michel's "type I" (Deisenhofer and Michel 1989): The transmembrane helical regions form bands

suggestive of membrane layers in a stack of two-dimensional crystals, with the membrane layers perpendicular to the *c* axis. The 2-fold screw axes along *a* and *b* are within the plane of the membrane and relate adjacent monomers with alternate up/down orientation in the membrane. The screw axis along *c* relates adjacent membrane layers. Protein in the membrane layer is quite tightly packed, and although only half the extrinsic domains go to each side of the membrane, because the extrinsic domains are wider than the membrane domains these layers are also well packed. As a result the extrinsic domains from adjacent membrane layers do not interdigitate but stack in such a way that each pair of adjacent membrane layers is separated by two layers of extrinsic domains. Moving up along the *c* axis, one passes through a membrane layer, then a layer of extrinsic domains of upwardly oriented molecules from that membrane, then a layer of extrinsic domains from downwardly oriented molecules in the next membrane, then that next membrane. The repeating unit consists of two membrane layers and four extrinsic layers, resulting in the long *c* axis of 291 Å.

The packing has also been determined for the $P2_12_12$ cell and is shown in figure 5b. Again there is a monomer in the asymmetric unit, and here also the membrane and extrinsic domains of the protein molecules line up in bands perpendicular to the long axis (***b*** in this case) suggesting stacks of two-dimensional crystals. The proper 2-fold axis is in the membrane plane and relates an up-down pair of adjacent molecules, which pack their membrane domains closely together (cyan and red molecules in Figure 5b). Otherwise packing in the membrane is rather loose (note the gap between the membrane domains of the red and brown molecules), and in this case the extrinsic domains from adjacent membranes interdigitate, with one 2-fold screw relating alternately the extrinsic domains of downwardly oriented molecules from the membrane above and upwardly oriented molecules from the membrane below. Dense packing in the extrinsic layers makes up for loose packing in the membrane, and V_m is slightly smaller for this form than for the first form. As a result of the interdigitation there is only one layer of extrinsic domains between each pair of adjacent membranes, and the long axis, which is again perpendicular to the membrane plane and includes two membranes, is shortened by about 90 Å to 201 Å. This should facilitate data collection, if this form can be routinely made to diffract to high resolution. In addition the different crystal contacts in the two crystals will help elucidate the effects of crystal contacts on the intrinsic structure in both forms, and if there are disordered regions in one form they may be clear in the other.

4. Conclusions. A procedure is presented for preparation of diffraction quality crystals of a vertebrate mitochondrial Respiratory Complex II. The crystals have the potential to diffract to at least 2.0 Å with optimization of post-crystal-growth treatment and cryoprotection. This should allow determination of the structure of this important and medically relevant membrane protein complex at near-atomic resolution, and provide great detail of the mode of binding of substrates and inhibitors at the two substrate-binding sites.

5. Acknowledgements- This work was supported by NIH grants GM62563 (NIGMS) and DK44842 (NIDDK). Lawrence Berkeley National Lab is operated by the Department of Energy, contract DE-AC03-76SF00098 to the University of California. Diffraction data were collected at the Advanced Light Source (ALS) at LBNL and at the Stanford Synchrotron Radiation Laboratory (SSRL), which is operated by the Department of Energy, Office of Basic Energy Sciences. The SSRL Biotechnology Program is supported by the National Institutes of Health, National Center for Research Resources, Biomedical Technology Program, and by the Department of Energy, Office of Biological and Environmental Research. We would like to thank Tzanko Doukov and Paul Ellis at SSRL and Corie Ralston, Christine Trame, and Azer Daz at the ALS for help with data collection.

6. References

- Ackrell, B.A. (2000) *FEBS Lett* **466**: 1-5
- Ackrell, B.A. (2002) *Mol Aspects Med* **23**: 369-84
- Albayrak, T., Scherhammer, V., Schoenfeld, N., Braziulis, E., Mund, T., Bauer, M.K., Scheffler, I.E. and Grimm, S. (2003) *Mol Biol Cell* **14**: 3082-96
- Baysal, B.E., Ferrell, R.E., Willett-Brozick, J.E., Lawrence, E.C., Myssiorek, D., Bosch, A., van der Mey, A., Taschner, P.E., Rubinstein, W.S., Myers, E.N., Richard, C.W., 3rd, Cornelisse, C.J., Devilee, P. and Devlin, B. (2000) *Science* **287**: 848-51
- Beal, M.F., Brouillet, E., Jenkins, B.G., Ferrante, R.J., Kowall, N.W., Miller, J.M., Storey, E., Srivastava, R., Rosen, B.R. and Hyman, B.T. (1993) *J Neurosci* **13**: 4181-92
- Berry, E.A. and Trumpower, B.L. (1987) *Anal Biochem* **161**: 1-15.
- Boardman, P.E., Sanz-Ezquerro, J., Overton, I., Burt, D., Bosch, E., Fong, W., Tickle, C., Brown, W., Wilson, S. and Hubbard, S. (2002) *Current Biology* **12**: 1965-1969
- Brunger, A.T., Adams, P.D., Clore, G.M., DeLano, W.L., Gros, P., Grosse-Kunstleve, R.W., Jiang, J.S., Kuszewski, J., Nilges, M., Pannu, N.S., Read, R.J., Rice, L.M., Simonson, T. and Warren, G.L. (1998) *Acta Crystallogr D Biol Crystallogr* **54**: 905-21
- Cecchini, G., Schroder, I., Gunsalus, R.P. and Maklashina, E. (2002) *Biochim Biophys Acta* **1553**: 140-57
- Cecchini, G. (2003) *Annu Rev Biochem* **72**: 77-109
- Davis, K.A. and Hatefi, Y. (1971) *Biochem Biophys Res Commun* **44**: 1338-44
- Deisenhofer, J. and Michel, H. (1989) *Embo J* **8**: 2149-70.
- Green, D.E., Whazton, D.C., Tsagoloff, A., Rieske, J.S. and Briexley, G.P. (1965). *Oxidase and Related Redox Systems*. King, T. E., Mason, H. S. a. and Morrison, M. New York, John Wiley. 2: 1032-1076
- Hagerhall, C. (1997) *Biochim Biophys Acta* **1320**: 107-41
- Ito, Y., Muraguchi, H., Seshime, Y., Oita, S. and Yanagi, S.O. (2004) *Mol Genet Genomics*
- Iverson, T.M., Luna-Chavez, C., Croal, L.R., Cecchini, G. and Rees, D.C. (2002) *J Biol Chem* **277**: 16124-30
- Lancaster, C.R. (2001) *FEBS Lett* **504**: 133-41
- Lancaster, C.R. (2003) *FEBS Lett* **555**: 21-8
- McDonnell, C.M., Benn, D.E., Marsh, D.J., Robinson, B.G. and Zacharin, M.R. (2004) *Clin Endocrinol (Oxf)* **61**: 510-514
- Niemann, S. and Muller, U. (2000) *Nat Genet* **26**: 268-70
- Otwinowski, Z. and Minor, W. (1997). *Macromolecular Crystallography, part A*. C.W. Carter, J. and Sweet, R. M. New York, Academic Press. 276: 307-326
- Oyedotun, K.S. and Lemire, B.D. (2004) *J Biol Chem* **279**: 9424-31
- Perrakis, A., Harkiolaki, M., Wilson, K.S. and Lamzin, V.S. (2001) *Acta Crystallogr D Biol Crystallogr* **57**: 1445-50

- Singer, T.P., Kearney, E.B. and Kenney, W.C. (1973) *Adv Enzymol Relat Areas Mol Biol* **37**: 189-272
- Smith, A.L. (1967) *Methods Enzymol.* **10**: 81-86
- Stroh, A., Anderka, O., Pfeiffer, K., Yagi, T., Finel, M., Ludwig, B. and Schagger, H. (2004) *J Biol Chem* **279**: 5000-7
- Thorne, R.E., Stum, Z., Kmetko, J., O'Neill, K. and Gillilan, R. (2003) *Journal of Applied Crystallography* **36**: 1455-1460
- Wikstrom, M.K. (1973) *Biochim Biophys Acta* **301**: 155-93
- Yankovskaya, V., Horsefield, R., Tornroth, S., Luna-Chavez, C., Miyoshi, H., Leger, C., Byrne, B., Cecchini, G. and Iwata, S. (2003) *Science* **299**: 700-4
- Yu, C.A. and Yu, L. (1980) *Biochim Biophys Acta* **591**: 409-20

7. Tables

Table 1. Data reduction statistics for complex II crystal. The data was collected at SSRL's beamline 9-1 on July 24, 2004, using the ADSC Quantum 315 detector (imaging surface 315 × 315 mm). In all 180° of data was collected in 0.25 degree oscillations. The crystal-to-detector distance was 400 mm, wavelength 0.979462 Å, and the exposure time was 10 s normalized for beam intensity. This particular crystal was from co-crystallization with excess oxaloacetate. A table of I/σ_I and R_{sym} vs resolution is included in supplemental materials for this paper.

Unit Cell Dimensions	70.01 x 84.40 x 289.50 Å
Solvent content	64 %
Matthew's coeff. V_M	3.47 Å ³ /Da
X-ray wavelength:	0.979462
Unique Reflections	78496
"Optical Resolution" ¹	1.76 Å
Wilson B-factor	41.0
Mosaicity	0.60°
Resolution Range, Å :	37.2 - 2.2 Å (2.27 - 2.19 Å)
Completeness:	86.6% (48%)
Data Redundancy:	4.4 (1.9)
R_{sym} on I :	0.116 (0.270)
$\langle I/\sigma_I \rangle$	11.8 (2.80)

1. Optical resolution- the smallest separation at which features are resolvable, calculated from native Patterson origin peak width by SFCHECK program (Vaguine et al. 1999).

8. Figure Captions

1. SDS-Polyacrylamide gel analysis at different stages during purification. Positions of molecular weight standards are indicated on the left, and the four subunits of Complex II are labeled on the right. Lane 1: Whole mitochondria. 2: Residue from detergent extraction. 3: Detergent extract. 4: Pooled fractions, TSK column. 5: Pooled flow-through fractions, hydroxyapatite column. 6: Pooled Fractions from DEAE-Sepharose elution. 7: Ammonium sulfate fractionation, 40% saturation pellet. 8: Pooled fractions from Sephacryl S-300 column. 9: Pooled fractions from glycerol density gradient centrifugation.

2. Absorption spectra of the purified avian Complex II preparation. Complex II was diluted to 6.8 μM in buffer containing 20 mM K-MOPS pH 7.5, 100 mM NaCl, 0.5 mM EDTA, 0.1 g/l dodecyl maltoside. A portion of this dilution was used to determine heme content from pyridine hemechrome spectra as described. Another portion was used directly to take spectra before (red) and after (black) reduction by a trace of solid dithionite. The difference (reduced minus oxidized) is plotted in magenta. The absorption scale has been normalized to read directly the extinction coefficient for the portion of the spectra beyond 470 nm. The region before 470 nm is plotted on a 4 \times reduced scale.

3. Typical crystals of Avian Complex II. (a) and (b) show crystals in two different wells. (c) shows crystals mounted in nylon loops on the goniometer at beamline 5.0.2, the ALS. See the text for description.

5. Crystal packing in the orthorhombic complex II crystals reveal them to be "type 1" crystals. In both crystal forms the cell contains four molecules. The crystal contains zones parallel to the a-b plane consisting of transmembrane helix regions, suggesting that the crystals are stacks of two-dimensional membrane crystals as described by Michel (his "type 1" crystals). Each such membrane zone has complex II molecules inserted alternately from opposite sides. (a) $P2_12_12_1$ crystals: The unit cell spans two such membranes, related by the two-fold screw axis along **c** (perpendicular to the membrane). Adjacent molecules within each membrane are related by the screw axes along **a** and **b**, as is often observed in two-dimensional crystals of membrane proteins. Between adjacent membrane zones are two zones of extrinsic domains, one from each membrane, resulting in the long c axis of this crystal form. (b) $P2_12_12$ crystals. The unit cell spans two membranes, related by the two-fold screw axis along **b**. The proper 2-fold axis is within the membrane plane, relating adjacent up- and down- oriented molecules such as the red and blue molecules depicted. Extrinsic domains from two adjacent membranes interdigitate, allowing the membranes to stack more closely and resulting in the shorter long axis of this crystal form. Along the c axis (perpendicular to the plane of the paper) there is only translational symmetry, that is, more molecules exactly behind those depicted.

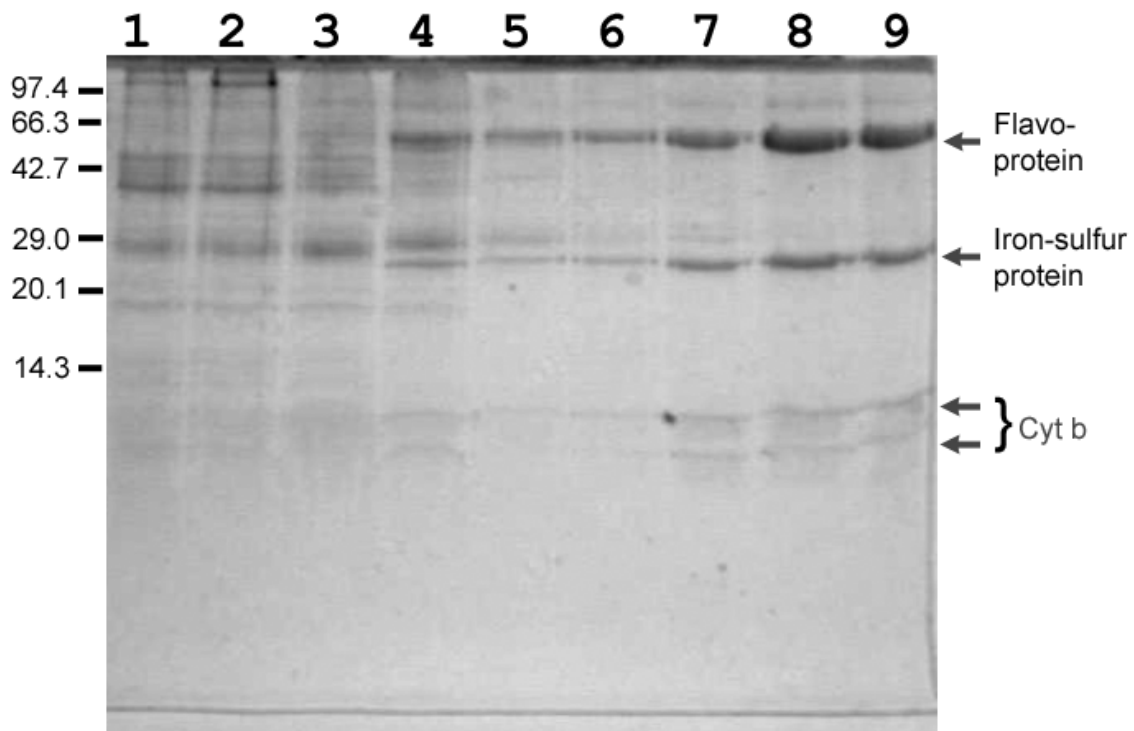


Figure 1, Huang et al.

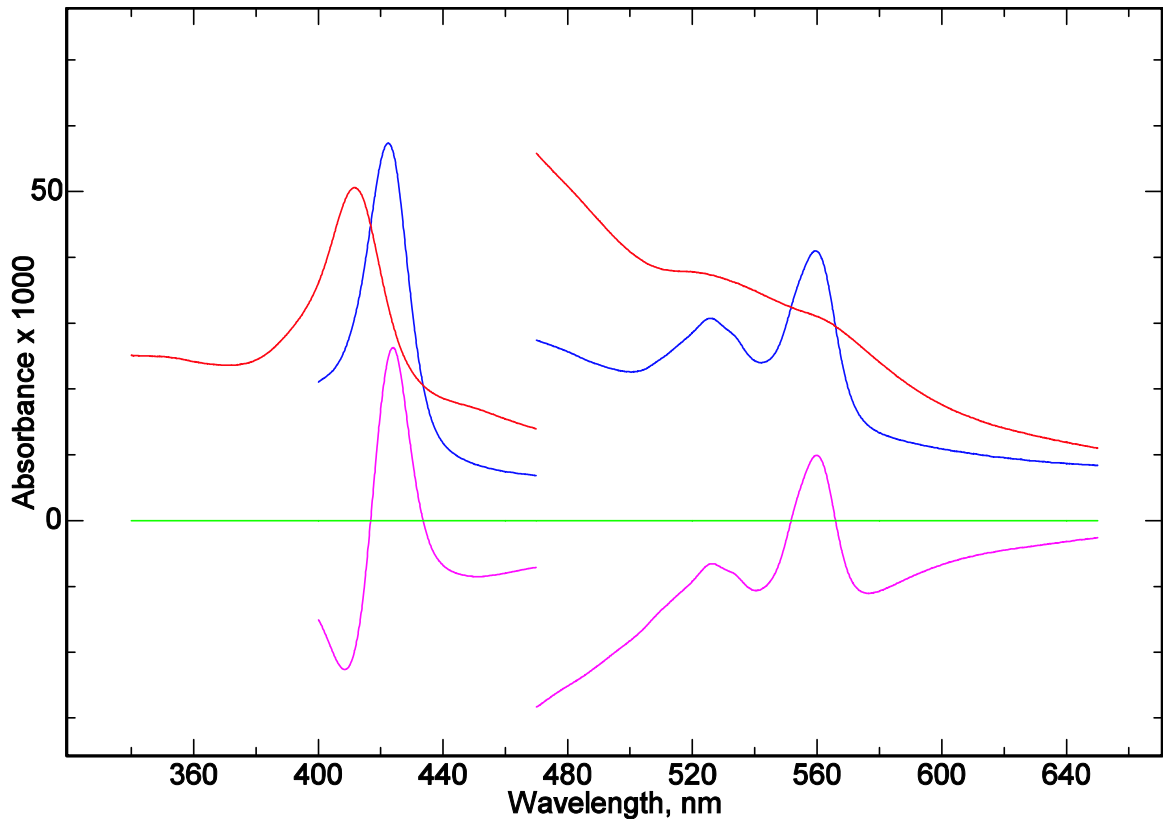


Figure 2, Huang et al.

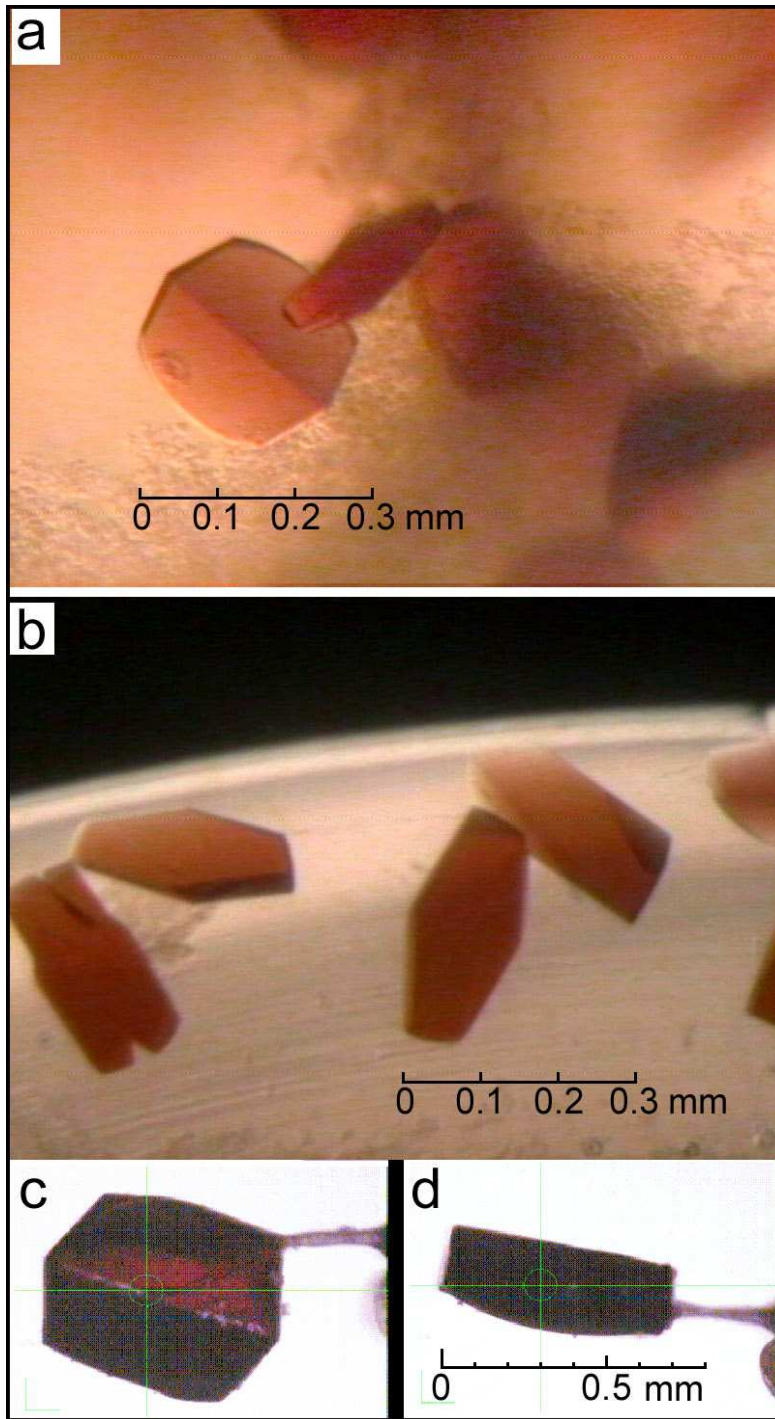


Figure 3, Huang et al.

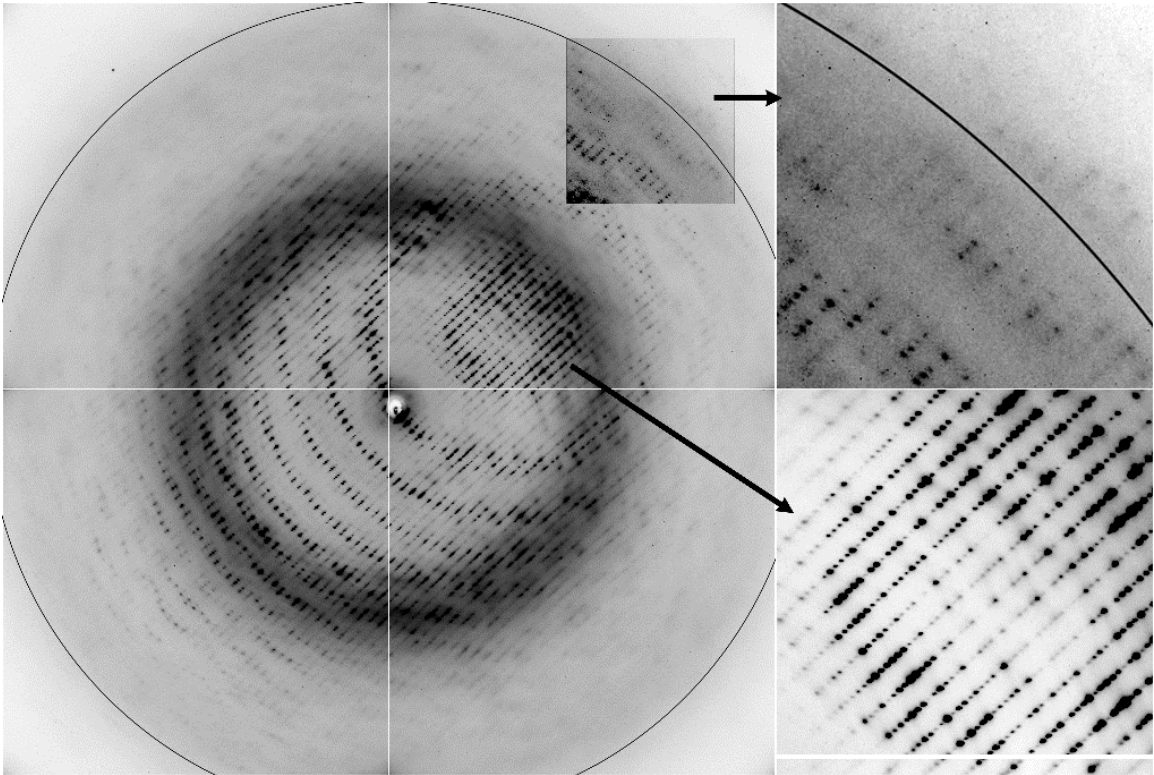
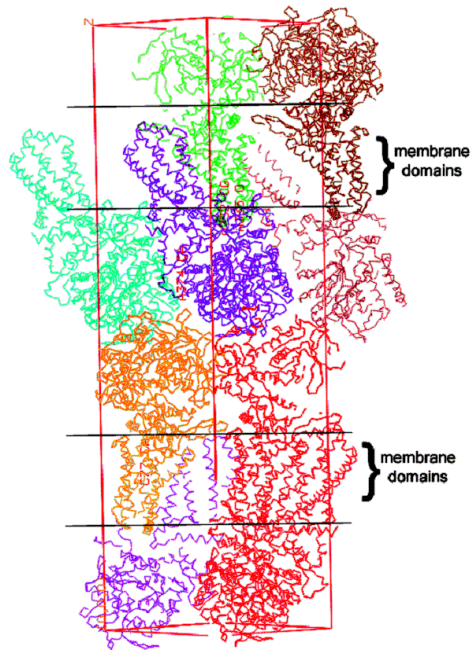


Figure 4, Huang et al.

a. $P2_12_12_1$



b. $P2_12_12$

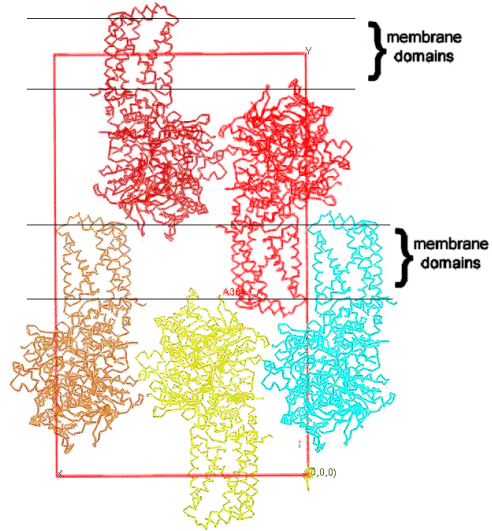


Figure 5, Huang et al.